

Precursor structure-determined fluorescence labeling for mesenchymal stem cells among four polyethylenimine-based carbon quantum dots

Bo Jiang^{a,1}, Cong Liu^{b,1}, Ying Guo^c, Hui Yang^b, Tian Sun^a, Yueyang Zhang^d, Kangxin Zhou^a,
Yong Guo^{c,*}, Hongwei Chen^{a,b,*}, Lingyun Sun^{b,*}

^a Department of Rheumatology and Immunology, The Affiliated Drum Tower Hospital of Nanjing University Medical School, Nanjing 210008, PR China

^b Nanjing Drum Tower Hospital, Clinical College of Traditional Chinese and Western Medicine, Nanjing University of Chinese Medicine, Nanjing 210008, PR China

^c Key Laboratory of Integrated Regulation and Resource Development on Shallow Lakes, Ministry of Education, College of Environment, Hohai University, Nanjing 210098, PR China

^d School of Basic Medicine and Clinical Pharmacy, China Pharmaceutical University, Nanjing 210009, PR China

ARTICLE INFO

Keywords:

Mesenchymal stem cells
Carbon quantum dot
Fluorescent imaging
Polyethylenimine
Linear precursor

ABSTRACT

A series of polyethylenimine (PEI)-based CQDs have been synthesized via a hydrothermal method by mixing linear PEI with linear citric acid (CA with COOH groups, PEICA), linear glucose (G with OH groups, PEIG), cyclic hyaluronic acid (HA with COOH groups, PEIHA) and cyclic boron nitride (BN with OH groups, PEIBN). PEICA had the best labeling effect ($100.00 \pm 0.26\%$) and the lowest cytotoxicity ($100.89 \pm 18.00\%$) for mesenchymal stem cells (MSCs), followed by PEIG ($91.83 \pm 7.60\%$; $92.84 \pm 5.56\%$), PEIHA ($84.34 \pm 7.87\%$; $61.27 \pm 11.34\%$) and PEIBN ($1.33 \pm 0.84\%$; $22.72 \pm 11.47\%$). The labeling effect of PEIHA for MSCs is lower than that of PEIG because the surface potential of PEIHA (6.58 mV) is higher than that of PEIG (0.50 mV). For PEIBN, it is likely that the precursor (BN) is less biocompatible than CA, HA and glucose. Thus, the linear acid (CA) is more appropriate to react with PEI for synthesizing CQDs with high labeling performance for MSCs. The control experimental results show that factors (such as surface potential, aromatic component, etc.) may all contribute to MSC labeling by PEICA. This work is helpful to design CQDs with high MSC labeling efficiency.

1. Introduction

Mesenchymal stem cells (MSCs) can differentiate into certain kinds of tissues [1,2] and regulate lymphocytes to improve immune imbalance, relieving many kinds of autoimmune diseases and repairing damaged tissues [3–5], such as myocardial infarction [6] and COVID-19 [7]. However, to date, how MSCs migrate to damaged organs and maintain their biological activity in the human body is still ambiguous and deserves much more attention. Clarifying this point is very helpful to promote the application of MSC therapy in the clinical treatment of patients.

To date, some methods have been developed to label MSCs to investigate their migration, distribution and active state in vivo. For example, magnetic materials (such as superparamagnetic iron oxide) have been combined with MSCs and further investigated with magnetic

resonance imaging methods [8,9]. Some organic chemicals (organic dyes, for instance) have good fluorescence performance and are used to track the migration and distribution of cells in the body [10,11]. Compared with organic dyes, carbon quantum dots (CQDs) contain light elements, such as C, O, N and H elements, which have better fluorescence performance, fluorescence stability and higher biocompatibility [12–17]. Thus, the labeling and imaging of cells has been a very significant application field for CQD since its discovery [13–19]. To date, some kinds of CQDs have been synthesized to track MSCs in vitro and/or in vivo (please see Table 1). For example, citric acid and ethylenediamine have been adopted as precursors to synthesize CQD for tracking and promoting the osteogenic differentiation of MSCs in vitro [20]. With betaine hydrochloride and tris(hydroxymethyl)aminomethane as the precursors, the as-synthesized CQD has both low cytotoxicity for MSCs (400 $\mu\text{g/ml}$) and good imaging performance for MSCs in

* Corresponding authors.

* Corresponding author at: Department of Rheumatology and Immunology, The Affiliated Drum Tower Hospital of Nanjing University Medical School, Nanjing 210008, PR China.

E-mail addresses: guoyong@hhu.edu.cn (Y. Guo), chenhw@nju.edu.cn (H. Chen), lingyunsun@nju.edu.cn (L. Sun).

¹ The authors made equal contributions to this paper.

<https://doi.org/10.1016/j.colsurfb.2022.112411>

Received 21 October 2021; Received in revised form 17 January 2022; Accepted 10 February 2022

Available online 11 February 2022

0927-7765/© 2022 Elsevier B.V. All rights reserved.

Table 1

The reported MSCs labeling by CQDs.

Carbon quantum dot (CQD)	MSC	Novelty	Publication
Using citric and ethylenediamine as precursor to synthesize CQD via hydrothermal method	Rat bone marrow mesenchymal stem cells (rBMSCs)	Tracking and promoting osteogenic differentiation of MSCs in vitro	Biomater Sci. 5(2017) 1820–1827 [20]
Using betaine hydrochloride and tris (hydroxymethyl) aminomethane as the precursors to synthesize CQD via hydrothermal method	Human adipose tissue-derived MSCs	Both low cytotoxicity for MSCs (400 µg/ml) and good imaging performance for MSCs in immunodeficient mice	Carbon. 152 (2019) 434–443 [21]
Using D-glucosamine hydrochloride and sodium pstyrenesulfonate as precursor to synthesize CQD via hydrothermal method	Rat bone MSCs	Labeling MSCs in vitro and promoting the osteogenic and chondrogenic differentiation of MSCs	J. Mater. Chem. B. 8 (2020) 5655–5666 [22]
Using diammonium citrate and spermidine as precursors to synthesize CQD via hydrothermal method	Human umbilical cord derived mesenchymal stem cells (hUCMSCs)	Investigating the relationship between surface charge of CQD and the MSC Labeling performance (also the MSC cytotoxicity) of CQD	Colloids Surf. B. 171(2018) 241–249 [23]

immunodeficient mice [21]. CQDs synthesized by using D-glucosamine hydrochloride and sodium pstyrenesulfonate as precursors can label MSCs in vitro [22]. It has been reported that CQDs with a positive surface are more appropriate to label MSCs than CQDs with a negative surface, but the positive charge on the CQD surface does not have a linear relationship with the.

labeling effect for MSCs since only relatively weak positive surface charges enabled CQDs to possess good biocompatibility and labeling efficiency, whereas a higher positive charge quantity will result in higher cytotoxicity [23]. However, the influence of the precursor structure on the labeling effect of CQD on MSCs is still not clear. Clarifying this point will be helpful to design CQDs with high labeling performance for MSCs.

Herein, to clarify the influence of the precursor structure on the labeling performance of MSCs, a series of CQDs (PEICA, PEIG, PEIHA, PEIBN, PEICA1, PEICA3, PEICA150, PEICA210, CA and G) have been synthesized with polyethylenimine (PEI), citric acid (CA), glucose (G), hyaluronic acid (HA) and boron nitride (BN) as precursors via a hydrothermal method. The labeling results show that PEICA has the best labeling effect ($100.00 \pm 0.26\%$) for MSCs, followed by PEIG ($91.83 \pm 7.60\%$), PEIHA ($84.34 \pm 7.87\%$) and PEIBN ($1.33 \pm 0.84\%$). Thus, the CQDs (PEICA and PEIG) formed by linear precursors (CA and Glucose) with PEI have better labeling performance for MSCs than that (PEIHA and PEIBN) from the cyclic precursors (HA and BN) with PEI. Furthermore, the CQD (PEICA) synthesized via the linear precursor with COOH groups (CA) and PEI has better labeling performance for MSC than that (PEIG) form the linear precursor with OH groups (glucose) with PEI. The labeling and cytotoxicity performance of PEI-based CQDs for MSCs may be influenced by many factors (such as surface potential and aromatic components), rather than is controlled by a single factor. This work has not been reported before and is helpful to design high-efficiency CQDs for MSC labeling for biomedical purposes.

2. Experimental section

2.1. Materials

All chemicals that were adopted to synthesize carbon quantum dots, including diboron trioxide (analytical grade), melamine (analytical grade), polyethylenimine (analytical grade), glucose (analytical grade), hyaluronic acid (analytical grade) and citric acid (analytical grade), were purchased from Yuanze Biotechnology Co., Ltd.

The reagents for cellular cultivation and labeling were obtained in the following way: ampicillin-streptomycin was purchased from HyClone (USA); DMEM/F-12 medium and fetal bovine serum (FBS) were obtained from Gibco (USA); propidium iodide (PI), RNase and paraformaldehyde were purchased from Sigma (USA); and a Cell Counting Kit-8 assay kit (CCK-8) was ordered from KeyGEN BioTECH (China).

2.2. Preparation of CQDs

PEICA CQD was prepared in the following procedure. Firstly, PEI solution was acquired by dissolving 0.2 g PEI in 20 ml deionized water; then, 0.1 g CA was weighed and put into the PEI solution to form a uniform mixed solution; after that, the mixed solution was put into the stainless steel high-pressure hydrothermal reactor and heated at 180 °C for 4 h in an oven; then, the solution in the hydrothermal reactor was removed with subsequent centrifugation (5000 r/min for 15 min) and dialysis (1000 kDa) for 24 h to remove the unreacted precursors and other impurities produced during the hydrothermal reaction process; finally, the dialyzed solution was freeze-dried to obtain the CQD sample, which was named PEICA.

Other PEI-based CQDs (PEIG, PEIHA and PEIBN) were synthesized in the same procedure as that of preparing PEICA, except that CA was replaced with glucose, hyaluronic acid and BN.

BN was synthesized in the same way as in our previous work [24]. Briefly, 24 g of melamine and 12 g of diboron trioxide were ground for half of an hour to acquire a mixture; then, the mixture was calcinated in a furnace at 1100 °C for 4 h with a heating rate of 10 °C/min; after that, the obtained BN sample was obtained with subsequent washing through the prepared hydrochloric acid (0.5 mol/L) and deionized water until the pH of the supernatant in the suspension was neutral; finally, the washed BN sample was dried in an oven at 60 °C for 10 h.

For a deep understanding of the labeling performance of PEI-based CQDs, a series of other CQDs were synthesized. The mass ratio between PEI and CA was 4:2 for PEICA, and the thermal temperature was 180 °C. The other two CQD samples were prepared at 180 °C by increasing the CA ratio to 4:3 and decreasing the CA ratio to 4:1. These two CQD samples were named PEICA1 and PEICA3. Another two CQD samples were prepared with the same mass ratio (4:2) between PEI and CA by increasing the thermal temperature to 210 °C and decreasing the thermal temperature to 150 °C. These two samples were named PEICA210 and PEICA150, respectively. The CQD with only CA as the precursor was synthesized at 180 °C and was named CA. The CQD with only glucose as the precursor was synthesized at 180 °C and was named G.

2.3. Characterizations of the synthesized CQDs

The zeta potential values of all the synthesized CQDs were determined using a potential analyzer (Zetasizer nano ZS, UK). The FTIR spectra of PEICA, PEIG and PEIHA were measured by a Fourier transform infrared (FTIR) instrument (Nexus 870, USA). XPS characterizations of all the synthesized CQDs were acquired using an X-ray photoelectron spectroscopy (XPS) instrument (PHI 5000 VersaProbe, Japan). The morphologies of PEICA, PEIG and PEIHA were obtained by transmission electron microscopy (TEM, JEM-200CX, Japan). The UV–vis diffuse reflectance spectra (UV-DRS) of PEICA, PEIG and PEIHA

were collected with a UV-vis spectrophotometer (Agilent CARY 100, USA). The fluorescent performance of PEICA, PEIG and PEIHA was investigated with an F-7000 fluorescence spectrophotometer (Hitachi, Japan).

2.4. Quantum yield measurement of the synthesized CQDs

The quinine method [25] was adopted to determine the quantum yield (Q) of the synthesized CQDs with quinine sulfate as the standard. The Q values of these CQDs were calculated with the following equation:

$$Q = Q_r \times \frac{I}{I_r} \times \frac{A_r}{A} \times \left(\frac{n}{n_r} \right)^2$$

where Q is the quantum yield, I is the measured integrated emission intensity, A is the optical density, and n is the refractive index of the solvent (1.33 for water). The subscript “r” referred to the reference standard with known QY.

2.5. Cell culture and cellular cytotoxicity experiment of the synthesized CQDs

Isolation and culture of human umbilical cord-derived mesenchymal stem cells (UC-MSCs) were described in our previous study [26]. The cytotoxicities of the synthesized CQDs in UC-MSCs were examined in vitro by using the CCK-8 assay kit. Generally, UC-MSCs were plated into 96-well plates at a density of 2.5×10^3 cells per well and then treated with the synthesized CQDs at concentrations of 0, 50, 100, 200, 400 or 800 $\mu\text{g ml}^{-1}$ for 24 or 48 h (or otherwise indicated). In addition, each sample was prepared in triplicates. Then, CCK-8 was added to each well

and incubated for 2 h at 37 °C with 5% CO₂ protected from light before the optical density (OD) value of each well was read by a microplate reader (BioTek Instrument, USA) at 450 nm. The wells with only cell culture medium with neither cells nor CQDs were set as the blank group. Cells without CQD treatment were used as the control group. The viability ratio of the control was set as 100%, and the viability ratio of the test group was calculated according to the formula $[(As-Ab)/(Ac-Ab)] \times 100\%$, where As was the OD value from the experimental cells, Ac was the OD value from the control cells and Ab was the OD value from the blank groups.

2.6. Cell labeling experiment of the synthesized CQDs

To obtain cell imaging, pictures of the UC-MSCs in culture with the synthesized CQDs at 0 h, 4 h, 8 h, 24 h and 48 h were taken by a live-cell-station microscope (Leica SP8, Germany) and recorded at three different fields at random for calculation of the ratio of labeled cells. To identify the cellular localization of CQDs in UC-MSCs, the cells were fixed with 4% paraformaldehyde, washed with phosphate-buffered saline (PBS, pH=7.4), and treated with PI (5 $\mu\text{g/ml}$) and RNase (20 $\mu\text{g/ml}$) for 10 min with a final PBS wash three times. Then, the cells were examined by a confocal laser scanning microscope (Nikon FV3000, Japan).

2.7. Statistical analysis

All data are shown as the mean \pm standard error of the mean. GraphPad Prime 8 software (GraphPad, USA) was used to analyze the data by one-way or two-way ANOVA. A p value < 0.05 was considered statistically significant.

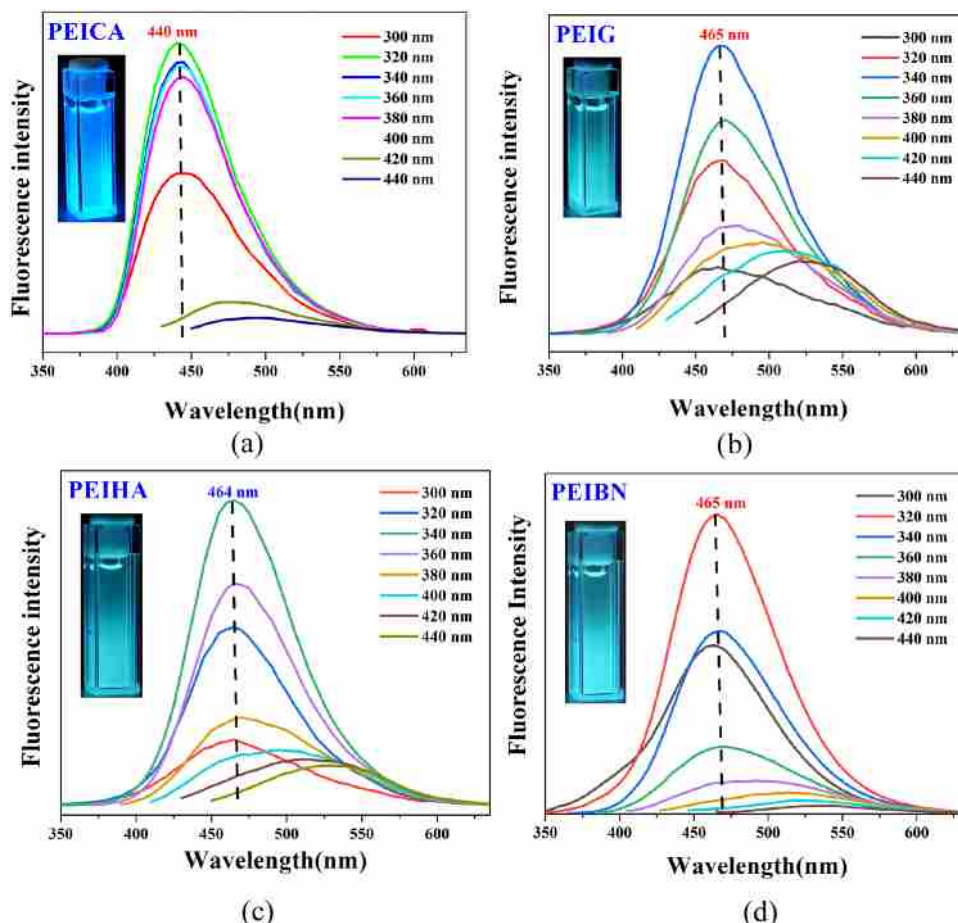


Fig. 1. (a) Fluorescence spectrum of PEICA; (b) fluorescence spectrum of PEIG; (c) fluorescence spectrum of PEIHA; (d) fluorescence spectrum of PEIBN.

3. Results and discussion

The fluorescence spectra of PEICA, PEIG, PEIHA and PEIBN were first investigated, and they all exhibited fluorescence performance under UV-light irradiation. From Fig. 1(a), the fluorescence spectra of PEICA can be classified into two parts: (1) one is wavelength-independent part (the excitation wavelength is less than 400 nm),

in which the wavelength of the emitting light is always approximately 440 nm (blue color) when the excitation wavelengths are 300 nm, 320 nm, 340 nm, 360 nm, 380 nm and 400 nm; (2) another part is the wavelength-dependent part (the excitation wavelength is larger than 400 nm), in which the wavelength of the emitting light increases with increasing excitation wavelength. For example, the wavelength of the emitting light is 470 nm when the excitation wavelength is 420 nm. The wavelength of the emitting light increases to 485 nm from 470 nm when the excitation wavelength increases from 420 nm to 440 nm (Fig. 1(a)). PEICA has the strongest emission peak at 440 nm (blue light) when the excitation wavelength is 320 nm. For comparison, the fluorescence performance of deionized water was also investigated. From Fig. S1, deionized water does not exhibit fluorescence performance when irradiated by UV light at 360 nm. Similar fluorescence phenomena were also found for PEIG, PEIHA and PEIBN (Fig. 1(b), (c) and (d)). For PEIG (Fig. 1(b)), its fluorescence performance is wavelength-independent when the excitation wavelength is less than 380 nm since the wavelength of the emitting light is always approximately 465 nm, whereas its fluorescence performance becomes wavelength-dependent when the excitation wavelength is larger than 380 nm (400 nm excitation \rightarrow 495 nm emission; 420 nm excitation \rightarrow 520 nm emission; 440 nm excitation \rightarrow 530 nm emission). For PEIHA (Fig. 1(c)), its fluorescence performance is wavelength-independent when the excitation wavelength is less than 380 nm since

the wavelength of the emitting light is always approximately 464 nm, whereas its fluorescence performance becomes wavelength-dependent when the excitation wavelength is larger than 380 nm (400 nm excitation \rightarrow 495 nm emission; 420 nm excitation \rightarrow 520 nm emission; 440 nm excitation \rightarrow 530 nm emission). For PEIBN (Fig. 1(d)), its fluorescence performance is wavelength-independent when the excitation wavelength is less than 360 nm since the wavelength of the emitting light is always approximately 465 nm, whereas its fluorescence performance becomes wavelength-dependent when the excitation wavelength is larger than 360 nm (380 nm \rightarrow 485 nm emission; excitation 400 nm excitation \rightarrow 515 nm emission; 420 nm excitation \rightarrow 520 nm emission; 440 nm excitation \rightarrow 529 nm emission). The strongest emission wavelengths for PEIG, PEIHA and PEIBN are all approximately 465 nm (green), and the corresponding excitation wavelengths are 340 nm, 340 nm and 320 nm, respectively (Fig. 1(b), (c) and (d)). This kind of fluorescence performance of PEICA, PEIG, PEIHA and PEIBN is different from that of some reported CQDs, which are all wavelength-dependent in the whole excitation wavelength range [22,27].

To understand the capability of the four PEI-based CQDs (PEICA, PEIG, PEIHA and PEIBN) to label MSCs, the CQDs were incubated with MSCs and examined at different time points afterwards. The experimental results show that only PEICA, PEIG, and PEIHA can efficiently label MSCs (Fig. 2). The fluorescence signals of PEICA, PEIG and PEIHA were all detected in.

cytoplasmic areas of MSCs, suggesting that PEICA, PEIG and PEIHA entered the cytoplasm of MSCs. However, different CQDs have distinct speeds of labeling MSCs. PEICA is the best marker of MSCs both rapidly and efficiently. A total of $91.07 \pm 7.16\%$ of MSCs were already successfully labeled by PEICA only in 4 h. The MSCs were comprehensively labeled within a subsequent period of 4 h (Fig. 2(a)). The second most prominent CQD labeling player was PEIG, the intake of which was

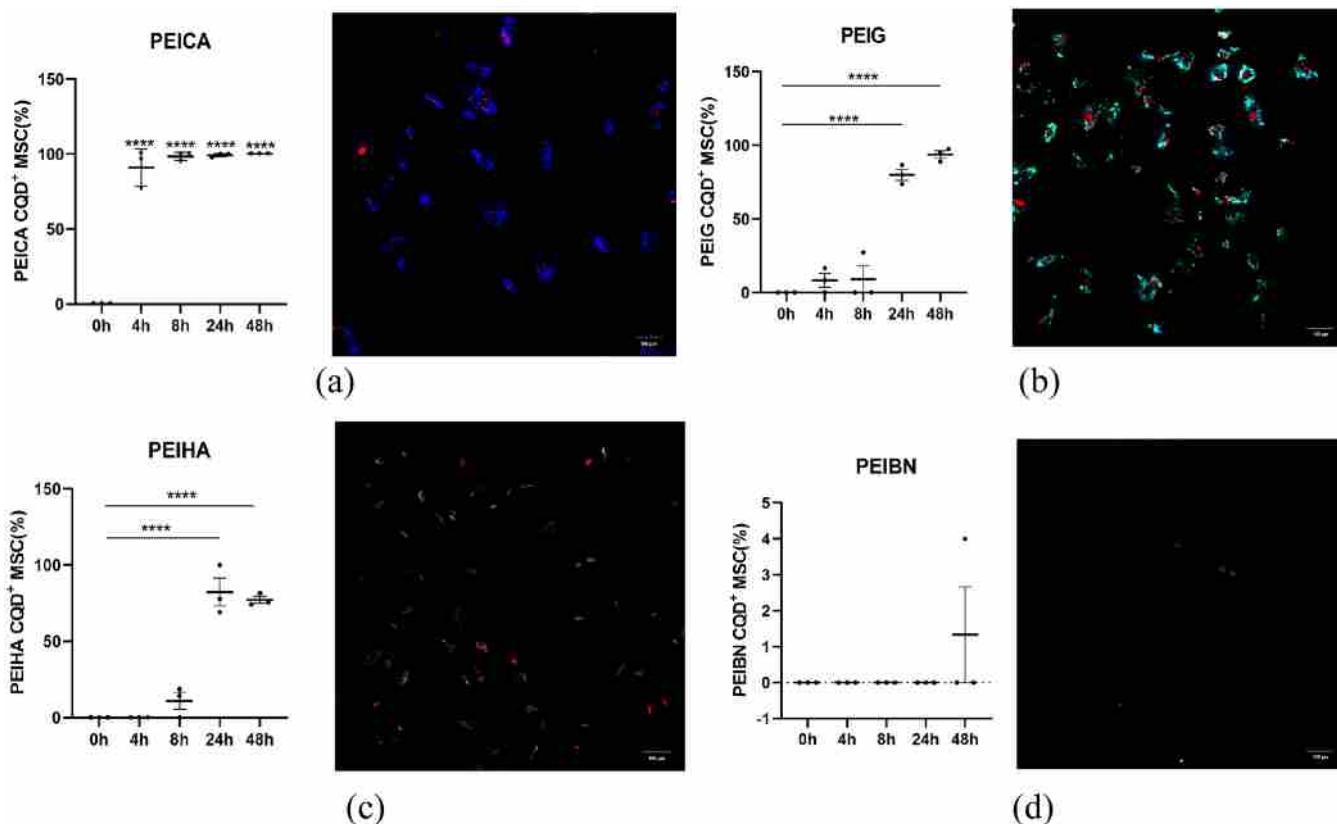


Fig. 2. Temporal labeling effects of PEICA, PEIG, PEIHA and PEIBN on MSCs. PEICA (a), PEIG (b), PEIHA (c), and PEIBN (d) Labeling effect of MSCs for 0 h, 4 h, 8 h, 24 h and 48 h (left) with a representative fluorescence image of MSCs at 48 h (right). Nuclei were stained with PI (red); scale bar, 100 μ m; n = 3; one-way ANOVA; *, $p < 0.05$; **, $p < 0.01$; ***, $p < 0.001$.

$8.33 \pm 7.10\%$ in 4 h (Fig. 2(b)). PEIHA labels MSCs much more slowly than PEICA and PEIG, with just $10.94 \pm 6.95\%$ of PEIHA⁺ MSCs observed in 8 h. The labeling efficiency of PEIBN for MSCs was just $1.33 \pm 0.84\%$ in 48 h. Overall, the first time points for CQD labeling at peak turns to be at 4 h, 8 h, 24 h and 48 h for PEICA, PEIG, PEIHA and PEIBN, respectively. Thus, it is assumed that crosstalk exists between CQDs and MSCs, controlling the on-off switch for the cells to recognize COD and authorize its passage through the cell membrane into the cytoplasm.

Then, the cytotoxicity and labeling effect of PEICA, PEIG, PEIHA and PEIBN on MSCs at different concentrations were investigated (Figs. 3 and 4). The results show that PEICA has the best labeling effect and biocompatibility for MSCs. Under 50–800 $\mu\text{g/ml}$ PEICA treatment, up to $100.00 \pm 0.26\%$ MSCs could be completely labeled at 24 h or 48 h (Fig. 3(a)). Meanwhile, the CCK-8 assay demonstrated that PEICA was not harmful to the MSCs at any concentration tested (Fig. 4(a)). For PEIG, it was sufficient to label MSCs efficiently starting at 50 $\mu\text{g/ml}$. The highest percentage of PEIG labeling was $91.83 \pm 7.60\%$ at 400 $\mu\text{g/ml}$ after 48 h (Fig. 3(b)). PEIG showed markedly toxic to MSCs at concentrations ranging from 400 $\mu\text{g/ml}$ to 800 $\mu\text{g/ml}$ (Fig. 4(b)). In contrast to PEIG and PEICA, even at the highest concentration of 400 $\mu\text{g/ml}$, PEIHA could label just $84.34 \pm 7.87\%$ of MSCs maximally in 48 h (Fig. 3(c)). However, under such conditions, only $61.27 \pm 11.34\%$ of MSCs survived, indicating that this concentration is toxic to MSCs. Cellular toxicity from PEIHA already occurred at 200 $\mu\text{g/ml}$ for MSCs after 48 h (Fig. 4(c)).

In contrast to the labeling performance of PEICA, PEIG and PEIHA for MSCs, PEIBN barely labeled MSCs (Fig. 3(d)). It is dramatically deleterious to MSCs at 100–800 $\mu\text{g/ml}$. Only $22.72 \pm 11.47\%$ of MSCs

remained variable after culture with MSCs and PEIBN for approximately 48 h (Fig. 4(d)). This is most likely because BN is one of the precursors to prepare PEIBN, and it is less biocompatible than glucose, hyaluronic acid and citric acid. In addition, the surface of PEIBN is highly positive (6.37 mV). It has been reported that CQDs with a high positive surface also have high toxicity to MSCs [23]. These two reasons may make PEIBN highly toxic and unable to label MSCs effectively. For a deep understanding of this point, time-lapse recording was performed with a live-cell station to capture the process of MSC labeling by PEIBN. Indeed, MSC labeling by PEIBN was successfully observed regardless of.

weak fluorescence intensity and very low efficiency ((Fig. S2 and Fig. 2(d)). However, once the MSCs were labeled with PEIBN, they struggled to survive with unhealthy morphology, started to die and floated in the culture soon, indicating the high toxicity of PEIBN to the cells. Thus, PEIBN can label MSC, However, its high cytotoxicity kills these labeled MSCs and decreases the labeling efficiency of PEIBN for MSCs. However, for PEICA, PEIG and PEIHA, why PEICA has the best labeling effect is still not clear. In the following, the surface potential, fluorescence stability, fluorescence quantum yield, fluorescence lifetime, size, surface functional groups and aromatic domain of PEICA, PEIG and PEIHA were investigated to clarify the factors influencing the labeling effect of PEICA, PEIG and PEIHA on MSCs.

The attachment of CQDs on the MSC surface is the precondition that CQDs can label MSCs. It has been reported that positive CQD is more appropriate to label MSCs than negative CQD [23]. Therefore, the surface potentials of PEICA, PEIG and PEIHA are determined to be 0.50 mV, 0.50 mV and 6.58 mV, respectively. PEICA and PEIG have the same surface potential, but they show different labeling effects for MSCs ($100.00 \pm 0.26\%$ vs $91.83 \pm 7.60\%$ for PEICA and PEIG, respectively)

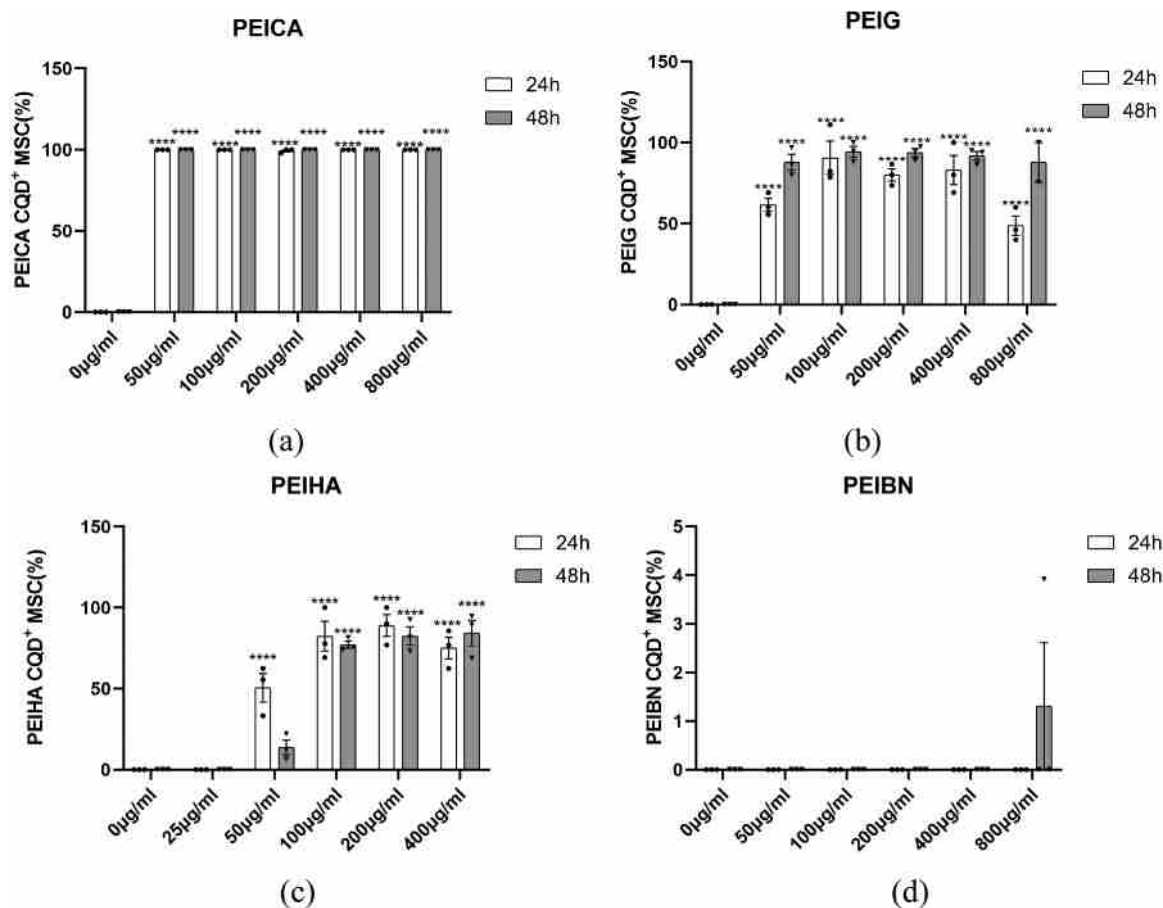


Fig. 3. Labeling effect of PEICA, PEIG, PEIHA and PEIBN on MSCs at different concentrations. Percentage of PEICA CQD+ (a), PEIG CQD+ (b), PEIHA CQD+ (c), and PEIBN CQD+ (d) MSCs incubated with PEICA, PEIG, PEIHA, and PEIBN at different concentrations for 24 h and 48 h. $n = 3$; two-way ANOVA, * * * *, $p < 0.0001$.

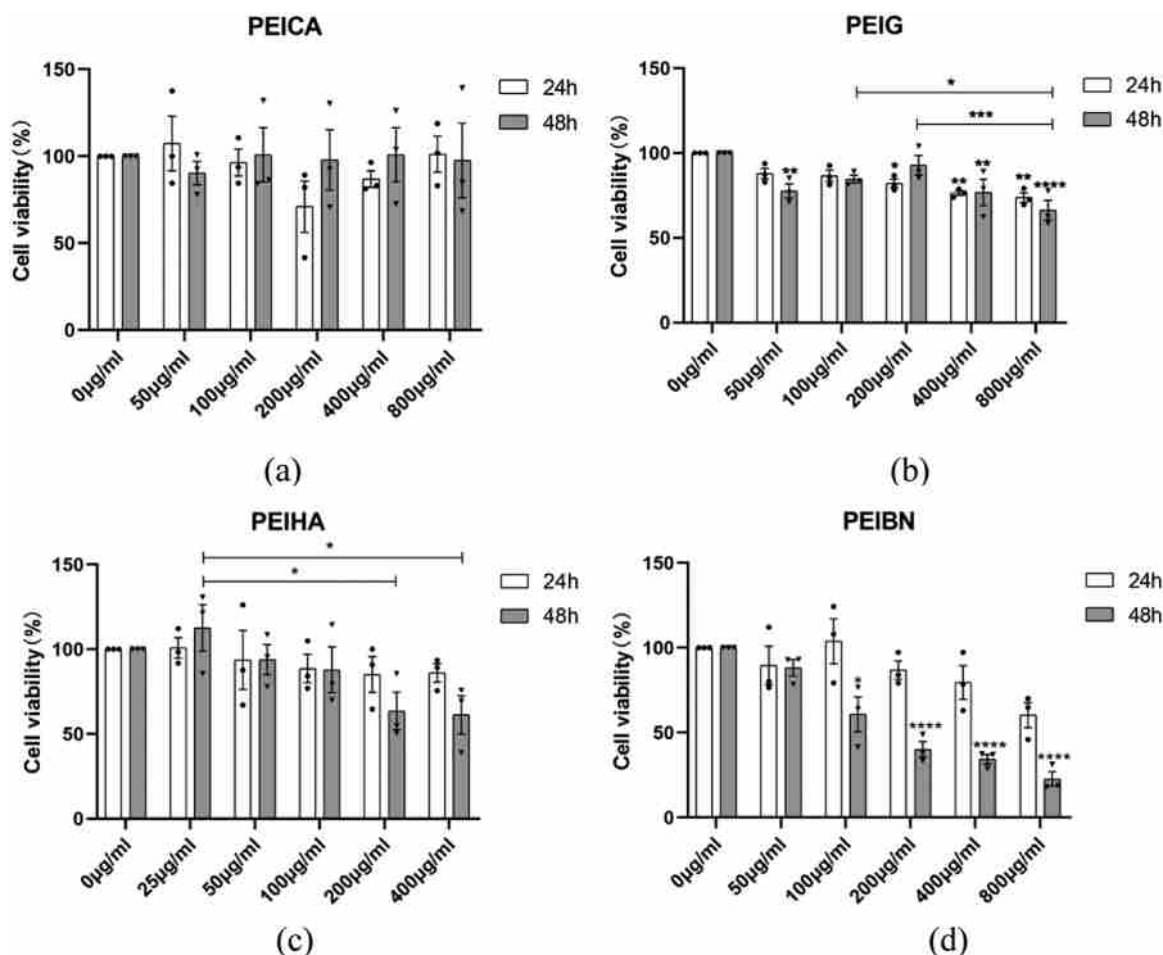


Fig. 4. Cytotoxicity tests for PEICA, PEIG, PEIHA and PEIBN in MSCs. MSC viability after treatment with PEICA (a), PEIG (b), PEIHA (c), and PEIBN (d) for 24 h and 48 h at different concentrations was examined by a CCK-8 kit. $n = 3$; two-way Anova analysis, *, $p < 0.05$.

(Fig. 3(a) and (b)). The surface potential of PEIHA is slightly larger than that of PEIBN (6.58 mV vs 6.37 mV). However, PEIHA could label MSCs ($84.34 \pm 7.87\%$), whereas PEIBN could not label MSCs at all (Fig. 3(c) and (d)). Thus, the surface potential is not the main reason that PEICA has the best labeling effect for MSCs among PEICA, PEIG and PEIHA. PEI is a polycationic polymer, and the positive electivity is from the protonation of these NH_2 and NH groups in PEI (please see Fig. 3(a)). The surface potentials of PEICA, PEIG, PEIHA and PEIBN are most likely determined by the residual and easily protonated groups (such as NH_2 and NH) on these CQD surfaces after PEI reacts with citric acid, hyaluronic acid, glucose and boron nitride (the structures of these precursors are shown in Fig. S3). To confirm this point, a series of PEICA CQDs were synthesized with different ratios between PEI and CA. For PEICA, the ratio between PEI and CA is 4:2, and the hydrothermal temperature is 180°C . Another two types of PEICA CQDs are synthesized under the same hydrothermal temperature (180°C) by increasing the ratio of PEI: CA to 4:3 and decreasing the ratio of PEI:CA to 4:1. They are named as PEICA3 and PEICA1, respectively. The residual NH_2 (or NH) groups in these PEICA CQDs will decrease with increasing quantity of CA. The obtained results showed that the surface potential of PEICA1 is 0.57 mV, followed by PEICA (0.50 mV) and PEICA3 (0.03 mV). Therefore, it is reasonable that the surface potential of CQDs is determined by these easily protonated groups (such as NH_2 and NH).

Fluorescence stability will determine if CQDs can label cells within a certain time scale. Therefore, the fluorescence stability of PEICA, PEIG and PEIHA was also studied to determine whether there was a relationship between the fluorescence stability and the labeling effect for MSCs. From Fig. S4(a), the fluorescence intensity at the starting time of

PEICA decreases to 99.9% two days later, 99.8% four days later, 99.7% six days later, 99.7% eight days later and 99.6% ten days later. For PEIG (Fig. S4(b)), its fluorescence intensity at the starting time decreased to 99.6% two days later, 99.3% four days later, 99.2% six days later, 99.0% eight days later and 99.0% ten days later. For PEIHA (Fig. S4(c)), its fluorescence intensity at the starting time decreased to 99.7% two days later, 99.7% four days later, 99.5% six days later, 99.5% eight days later and 99.5% ten days later. The difference among the fluorescence stabilities of PEICA, PEIG and PEIHA is too small since they are all above 99.0% within ten days. Thus, fluorescence stability is not the reason that PEICA has the best labeling effect for MSCs among PEICA, PEIG and PEIHA.

Based on reported works [20–23] and labeling experiments (Fig. 2), MSCs are labeled by the entry of CQDs into the cytoplasm in MSCs. This means that the size of CQDs may also have some relationship with the labeling effect for MSCs since these CQDs will enter MSCs through their membranes. The size of PEICA ranges from 2 nm to 10 nm, and the average size of PEICA is 5.87 nm. From Fig. 5(a), the size of PEICA at approximately 6 nm has the largest ratio: 45%, followed by that at approximately 4 nm (25%), that at approximately 8 nm (17%), that at approximately 2 nm (10%) and that at approximately 10 nm (3%). For PEIG (Fig. 5(b)), its largest size ratio is approximately 4 nm (43%), followed by 2 nm (35%), 6 nm (15%), 8 nm (6%) and 10 nm (1%). The average size of PEIG is 4.13 nm. For PEIHA (Fig. 5(c)), its largest size ratio is approximately 4 nm (48%), followed by 2 nm (25%), 6 nm (17%), 8 nm (8%) and 10 nm (2%). The average size of PEIHA is 4.58 nm. For PEIG and PEIHA, the largest size ratios (43% and 48%) are all approximately 4 nm, while the largest size ratio (45%) of PEICA is

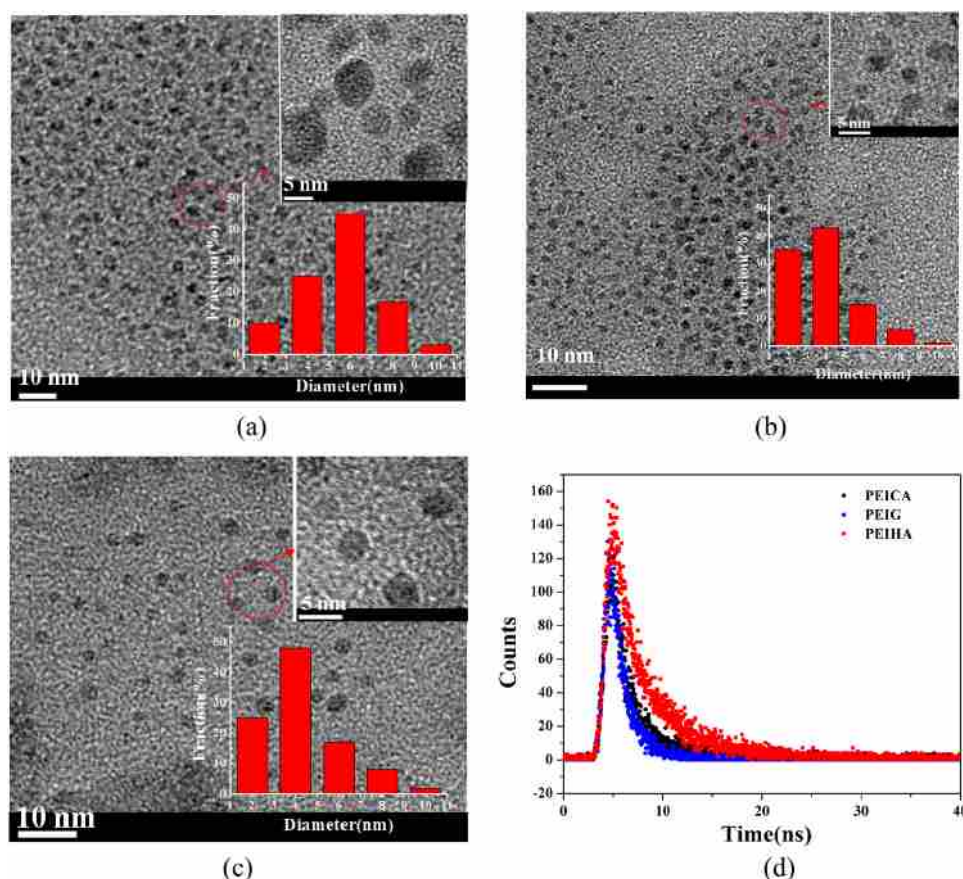


Fig. 5. (a) HRTEM image and size analysis of PEICA; (b) HRTEM image and size analysis of PEIG; (c) HRTEM image and size analysis of PEIHA; (d) fluorescence lifetime of PEICA, PEIG and PEIHA.

approximately 6 nm. However, PEICA had the best labeling effect ($100.00 \pm 0.26\%$), followed by PEIG ($91.83 \pm 7.60\%$) and PEIHA ($84.34 \pm 7.87\%$). Therefore, it is likely that size is not the determining factor that PEICA has the best labeling effect for MSCs among the three PEI-based CQDs. In other words, all three CQDs (PEICA, PEIG and PEIHA) are small enough to enter MSCs through the plasma membrane. In addition, the strongest fluorescence peak of PEICA.

is at 440 nm (Fig. 1(a)), whereas the strongest fluorescence peaks of PEIG and PEIHA are all at approximately 465 nm (Fig. 1(b) and (c)). Thus, the size may influence the fluorescence peaks of these PEI-based CQDs.

The fluorescence lifetimes of PEICA, PEIG and PEIHA were also investigated since CQDs with a long fluorescence lifetime may have a longer time to emit light. From Fig. 5(d), PEIHA has the longest fluorescence time (3.1 ns), followed by PEICA (1.7 ns) and PEIG (1.5 ns). The fluorescence lifetime of PEICA is longer than that of PEIG (1.7 ns vs 1.5 ns) but is shorter than that of PEIHA (1.7 ns vs 3.1 ns). PEICA had the best labeling effect for MSCs ($100.00 \pm 0.26\%$), followed by PEIG ($91.83 \pm 7.60\%$) and PEIHA ($84.34 \pm 7.87\%$). This suggests that the fluorescence lifetime is also not the determining factor resulting in the best labeling effect of PEICA for MSCs among the three CQDs.

A high fluorescence quantum yield usually means that using fewer CQDs can acquire a high emission effect. Thus, the fluorescence quantum yields of PEICA, PEIG and PEIHA were also investigated, which were 9.9%, 5.9% and 6.9%, respectively (Table S1). PEICA has the highest fluorescence quantum yield (9.9%) and the best labeling effect for MSCs. The fluorescence quantum yield of PEIG was lower than that of PEIHA (5.9% vs 6.9%), while the labeling effect of PEIG for MSCs was better than that of PEIHA ($91.83 \pm 7.60\%$ vs $84.34 \pm 7.87\%$ for PEIG and PEIHA, respectively). This may be because the surface potential of

PEIHA (6.58 mV) is higher than that of PEIG (0.50 mV), which results in the higher cytotoxicity [23] and the lower labeling effect of PEIHA, with approximately 40% more cell loss and 10% less cell labeling efficiency (Fig. 3(b), (c) and Fig. 4(b), (c)). It has been reported that CQDs with a positive surface are more appropriate to label MSCs than CQDs with a negative surface, but the weak positive surface enables CQDs to possess good biocompatibility and labeling efficiency, whereas the higher positive surface will result in higher cytotoxicity [23]. Thus, the fluorescence quantum yield may be related to PEICA having the best labeling effect for MSCs among the three CQDs.

It is well known that structure has a very significant relationship with the performance of materials. To clarify why PEICA has the best labeling effect for MSCs, the surface structures of PEICA, PEIG and PEIHA were investigated via FTIR, UV-Vis and XPS spectra. From Fig. S5(a), the peak at $\sim 3425 \text{ cm}^{-1}$ is likely from the contribution of O-H and N-H stretching models [28]; the peaks at 2930 cm^{-1} and 2940 cm^{-1} originate from the contribution of C-H [24,25]; and the peaks at 1715 cm^{-1} , 1633 cm^{-1} and 1558 cm^{-1} are attributed to the vibrations of C=O and C=C, respectively [29,30]. From the FTIR spectra of PEICA, PEIG and PEIHA, the FTIR spectrum of PEIG is nearly identical to that of PEIHA, suggesting that PEIG and PEIHA have similar functional groups. The FTIR spectrum of PEICA is also similar to that of PEIG and PEIHA, except for the FTIR peaks between 1700 cm^{-1} and 1500 cm^{-1} (Fig. S5(a)). The FTIR peaks in the region were mainly related to the C=C and C=O bonds [28,29]. Thus, it is very likely that the C=C or C=O region in CQD may be related to why PEICA has the best labeling effect for MSCs among PEICA, PEIG and PEIHA.

The UV-Vis spectra of PEICA, PEIG and PEIHA are shown in Fig. S5 (b). PEICA has two absorption UV-Vis peaks: one peak is at 239 nm, which is attributed to the electron transition from the π orbital to the

π^* orbital of the polycyclic aromatic domain in PEICA [28], and another peaks at 352 nm, which is from the $n-\pi^*$ transition of C-N [31,32]. PEIG and PEIHA have only one obvious UV-Vis peak at approximately 360 nm (PEIG: 362 nm and PEIHA: 352 nm), which is also most likely from the $n-\pi^*$ transition of C-N [31,32]. Based on the UV-Vis spectra of PEICA, PEIG and PEIHA, PEICA can absorb light with shorter wavelengths than PEIG and PEIHA since PEICA has obvious absorption peaks at both 239 nm and 352 nm, while PEIG and PEIHA have obvious absorption peaks at only 362 nm and 352 nm, respectively. Thus, PEICA can theoretically emit light with shorter wavelengths than PEIG and PEIHA. This is consistent with the fluorescence results since PEICA emits blue light and PEIG and PEIHA emit green light under UV light irradiation (Figs. 1 and 2). Furthermore, based on the UV-Vis spectra, only PEICA contains an obvious aromatic domain ($\pi-\pi$ domain) since the absorption peak at 239 nm is attributed to the electron transition from the π orbital to the π^* orbital of the polycyclic aromatic domain in CQDs [28,31]. It is well known that the main component of the cell membrane is phospholipids, which are amphiphilic biomolecules with both hydrophilic and hydrophobic parts [33,34]. PEICA has hydrophilic surface functional groups (OH, C-O, C=O, etc.), which can make PEICA uniformly disperse in water (Fig. S6(a)). It is also true for PEIG and PEIHA (Fig. S6 (b) and (c)). However, PEICA has an obvious aromatic domain ($\pi-\pi$ domain), which makes PEICA hydrophobic. Thus, PEICA may have a better amphiphilic performance than PEIG and PEIHA. In summary, it is most likely that the aromatic domain ($\pi-\pi$ domain) is related to the high labeling effect of PEICA for MSCs based on the FTIR and UV-Vis results of PEICA, PEIG and PEIHA. In recent reports using CQDs to label MSCs [20–22], those CQDs all have aromatic domains since they all have UV-Vis absorption peaks between 200 nm and 300 nm, which are from the electron transition from the π orbital to the π^* orbital of the polycyclic aromatic domain in CQDs.

To further confirm that PEICA has a more aromatic domain ($\pi-\pi$ domain) than PEIG and PEIHA, the XPS method was adopted to investigate the valence state of C elements in PEICA, PEIG and PEIHA. According to Fig. S7(a), PEICA contains 61.40% carbon, 22.18% nitrogen and 16.43% oxygen. The carbon, nitrogen and oxygen contents in PEIG are 63.92%, 25.94%, and 10.13%, respectively (Fig. S7(b)), while those in PEIHA are 65.20%, 26.01%, and 8.79%, respectively (Fig. S7(c)). Due to their high nitrogen content, PEICA, PEIG and PEIHA are all nitrogen-rich CQDs [28,35,36]. From the C1s spectra of PEICA, PEIG and PEIHA (Fig. S5(c), (d) and (e)), they all have C1s peaks at 284.1 eV, 284.4 eV, 285.6 eV, 286.6 eV and 287.6 eV, which are attributed to C=C, C-C, C-N, C-O and C=O, respectively [20–22,34–36]. By comparing the C1s peak of C=C (sp^2 C, 284.1 eV) in Fig. S5(c), (d) and (e), the C1s peak of C=C (sp^2 C) of PEICA is more obvious than that of PEIG and PEIHA. It has been reported that the percent of different bonds (C=C, C-C, C-N, etc.) in C1s spectra can be acquired based on XPS data by the ratio between the sub-peak area and C1s area in C1s spectra [37]. Herein, the percentages of C=C (sp^2 carbon) and C-C (sp^3 carbon) in C1s spectra of PEICA, PEIG and PEIHA were calculated. From Fig. S5(f), the percentages of C=C (sp^2 C) and C-C (sp^3 C) in the C1s spectra of PEICA are 28.1% and 11.2%, respectively; for PEIG, the percentages of C=C (sp^2 carbon) and C-C (sp^3 C) are 18.9% and 33.5%, respectively; and for PEIHA, the percentages of C=C(sp^2 C) and C-C (sp^3 C) are 21.2% and 27.0%, respectively. The percent (28.1%) of C=C (sp^2 C) in the C1s spectrum of PEICA is obviously higher than that (18.9%) of PEIG and

that (21.2%) of PEIHA, suggesting that PEICA has a more aromatic component (sp^2 C) than PEIG and PEIHA. Thus, it seems that the aromatic component ($\pi-\pi$ domain) is related to the high labeling effect of PEICA for MSCs. The labeling effect of PEIG for MSCs is better than that of PEIHA because the surface potential (6.58 mV) of PEIHA is higher than that (0.50 mV) of PEIG, and PEIHA has higher cytotoxicity than PEIG [23].

To better understand whether the aromatic component (sp^2 C) is the main factor influencing the labeling performance of PEICA for MSCs, a series of CQDs have been synthesized. For PEICA, the ratio between PEI

and CA is 4:2, and the hydrothermal temperature is 180 °C. Two types of PEICA CQDs are synthesized under the same hydrothermal temperature (180 °C) by increasing the ratio of PEI:CA to 4:3 and decreasing the ratio of PEI:CA to 4:1. They are named as PEICA3 and PEICA1, respectively. From Fig. 6(a) and (b), MSCs can be effectively labeled by PEICA1 (200 μ g/ml – 800 μ g/ml), PEICA (50 μ g/ml – 800 μ g/ml) and PEICA3 (50 μ g/ml – 800 μ g/ml). But PEICA3 has the obvious cytotoxicity for MSC (50 μ g/ml – 800 μ g/ml). In summary, PEICA has the best effect related to PEICA3 and PEICA1.

Then, two other types of PEICA CQDs are further synthesized under the same ratio (4:2) between PEI and CA by increasing the hydrothermal temperature to 210 °C and decreasing the hydrothermal temperature to 150 °C. They are named PEICA210 and PEICA150, respectively. The labeling and cytotoxicity experiments of these PEICA CQDs for MSC are shown in Fig. 6(c) and (d). MSCs can be effectively labeled by PEICA150 (50 μ g/ml – 800 μ g/ml), PEICA (50 μ g/ml – 800 μ g/ml) and PEICA210 (400 μ g/ml – 800 μ g/ml). But PEICA150 has the obvious cytotoxicity for MSC (50 μ g/ml – 800 μ g/ml). In summary, PEICA also shows the best labeling and cytotoxicity performance related to PEICA210 and PEICA150.

Furthermore, another two CQDs were produced with CA and glucose as precursors by using the same procedure of synthesizing PEICA. The two CQDs are named CA and G. Their labeling effects for MSCs are shown in Fig. S8. It is obvious that neither CA nor G alone can efficiently label MSCs. However, PEICA and PEIG can label MSC well.

For deep understanding the above labeling and cytotoxicity results of PEICA1, PEICA, PEICA3, PEICA150, PEICA210, CA and G, their aromatic component, surface potential and fluorescence quantum yield have been characterized and listed in Table S2. From Fig. 6(a) and (b), PEICA1, PEICA and PEICA3 all have good labeling performance for MSC, but just PEICA3 has the obvious cytotoxicity for MSC (50 μ g/ml – 800 μ g/ml). There are no linear relationship can be found between the cytotoxicity and aromatic component, surface potential, fluorescence quantum yield. From Fig. 6(c) and (d), PEICA150, PEICA and PEICA210 all have good labeling performance for MSC, but just PEICA150 has obvious cytotoxicity for MSC even at the exposure concentration of 50 μ g/ml, this may due to that the surface potential (3.55 mV) PEICA150 is obvious higher than that of PEICA (0.50 mV) and PEICA210 (−0.07 mV) since high positive surface will make the high cytotoxicity of CQD for MSC [23]. However, the surface potential of PEICA210 is −0.07 mV and it can still effectively label MSC. For CA and G (Fig. S6 and Table S2), they can not label MSC even the ratio of aromatic components (sp^2 C) in them (40.1% in CA and 31.3% in G) are higher than that (28.1%) in PEICA. Thus, the labeling and cytotoxicity performance of PEI-based CQDs for MSC may be influenced by many factors (such as surface potential, aromatic component, etc.), rather than is controlled by a single factor.

4. Conclusion

In this work, a series of CQDs (PEICA, PEIG, PEIHA, PEIBN, PEICA1, PEICA3, PEICA150, PEICA210, CA and G) were synthesized to clarify the influence of the precursor structure on their labeling performance for MSCs. Based on the labeling and toxicity results, the CQDs (PEICA and PEIG) formed by linear precursors (CA and glucose) with PEI have better labeling performance for MSCs than the CQDs (PEIHA and PEIBN) produced from cyclic precursors (HA and BN) with PEI. Furthermore, the CQD (PEICA) synthesized via the linear precursor with COOH groups (CA) and PEI has better labeling performance for MSC than that (PEIG) from the linear precursor with OH groups (Glucose) with PEI. The labeling and cytotoxicity performance of PEI-based CQDs for MSCs may be influenced by many factors (such as surface potential and aromatic components), rather than is controlled by a single factor. This work is helpful to design high-efficiency CQDs for MSC labeling and promote the application of CQDs in MSC labeling for biomedical purposes.

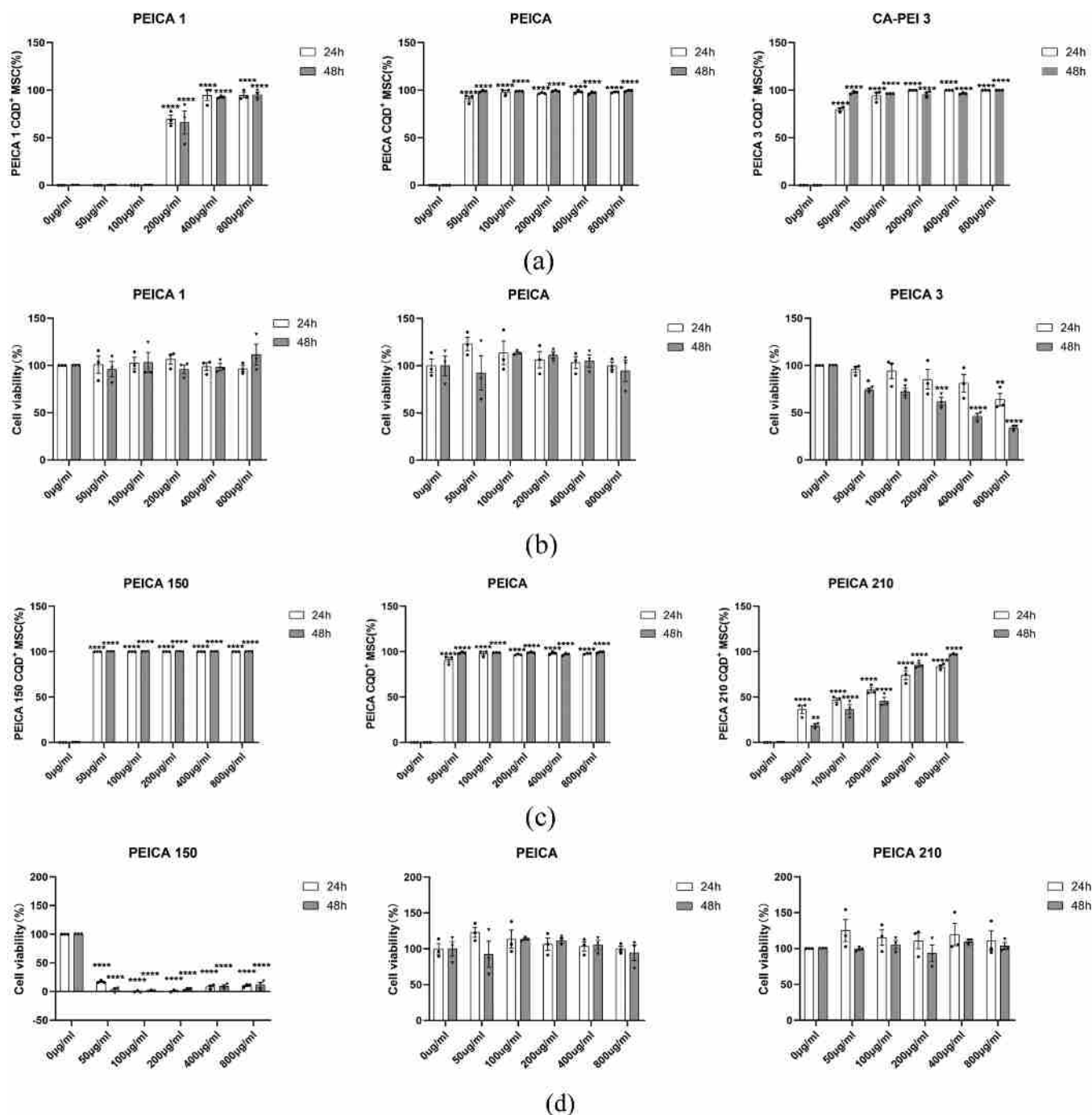


Fig. 6. MSC labeling effects (a) and cytotoxicity tests (b) of PEICA1, PEICA and PEICA3; MSC labeling effects (c) and cytotoxicity tests (d) of PEICA150, PEICA and PEICA210. $n = 3$; Two-way Anova analysis; ***, $p < 0.0001$.

Supporting Information

The fluorescence stability test of PEICA, PEIG and PEIHA; the parameters for calculating the quantum yield of PEICA, PEIG and PEIHA; the images of PEICA, PEIG and PEIHA; and the XPS spectra of PEICA, PEIG and PEIHA are all provided in the [Supporting information](#).

CRediT authorship contribution statement

Bo Jiang: Conceptualization, Methodology, Writing – original draft. **Cong Liu:** Methodology, Validation, Writing – original draft. **Ying Guo:** Resources. **Hui Yang:** Data Curation. **Tian Sun:** Data Curation.

Yueyang Zhang: Data Curation. **Kangxin Zhou:** Data Curation. **Yong Guo:** Visualization, Project administration. Funding acquisition. **Hongwei Chen:** Visualization, Funding acquisition. **Lingyun Sun:** Visualization, Supervision, Funding acquisition.

Declaration of Competing Interest

The authors declare that they have no known competing financial interests or personal relationships that could have appeared to influence the work reported in this paper.

Acknowledgments

This work was supported by Nanjing Science and Technology Development Plan (201715021), PANDA Project 2018-Clinical Research Special Fund of China Foundation for International Medical Exchange (Z-2014-06-2-1863), the Fundamental Research Funds for the Central Universities (B210203040), Key Project supported by Medical Science and Technology Development Foundation, Nanjing Department of Health (ZKX18011 and ZKX20019), and National Natural Science Foundation of China (81871319).

Appendix A. Supporting information

Supplementary data associated with this article can be found in the online version at [doi:10.1016/j.colsurfb.2022.112411](https://doi.org/10.1016/j.colsurfb.2022.112411).

References

- [1] M. Mendt, K. Rezvani, E. Shpall, Mesenchymal stem cell-derived exosomes for clinical use, *Bone Marrow Transpl.* 54 (2019) 789–792, <https://doi.org/10.1038/s41409-019-0616-z>.
- [2] A.K. Gundestrup, C.D. Lynggaard, L. Forner, T.J. Heino, C.V. Buchwald, Mesenchymal stem cell therapy for osteoradionecrosis of the mandible: a systematic review of preclinical and human studies, *Stem Cell Res. Rep.* 16 (2020) 1208–1221, <https://doi.org/10.1007/s12015-020-10034-5>.
- [3] G.P. Donald, F.P. Mark, Concise review: MSCs-derived exosomes for cell-free therapy, *Stem Cells* 35 (2017) 851–858, <https://doi.org/10.1002/stem.2575>.
- [4] S.G. Xu, C. Liu, H.L. Ji, Concise review: therapeutic potential of the mesenchymal stem cell derived secretome and extracellular vesicles for radiation-induced lung injury: progress and hypotheses, *Stem Cell Transl. Med.* 8 (2019) 344–354, <https://doi.org/10.1002/sctm.18-0038>.
- [5] M.E.J. Reinders, M.J. Hoogduijn, Nk cells and MSCs: possible implications for MSCs therapy in renal transplantation, *J. Stem Cell Res. Ther.* 4 (2014), 1000166, <https://doi.org/10.4172/2157-7633.1000166>.
- [6] E.J. Wright, N.W. Hodson, M.J. Sherratt, K. Moustapha, A.L. Lewis, W. Christine, M. Nadim, C.M. Holt, Combined MSCs and GLP-1 therapy modulates collagen remodeling and apoptosis following myocardial infarction, *Stem Cells Int.* 2016 (2016), 7357096, <https://doi.org/10.1155/2016/7357096>.
- [7] Y.J. Cao, H.Y. Wu, W.L. Zhai, Y. Wang, M.D. Li, M. Li, L. Yang, Y. Tian, Y.H. Song, J. Li, Y.Y. Wang, Q. Ding, L.Q. Zhang, M. Cai, Z.J. Chang, A safety consideration of mesenchymal stem cell therapy on COVID-19-sciencedirect, *Stem Cell Res.* 49 (2020), 102066, <https://doi.org/10.1016/j.scr.2020.102066>.
- [8] S.L. Hu, P.G. Lu, L.J. Zhang, F. Li, Z. Chen, N. Wu, H. Meng, J.K. Lin, H. Feng, In vivo magnetic resonance imaging tracking of SPIO-labeled human umbilical cord mesenchymal stem cells, *J. Cell Biochem.* 113 (2012) 1005–1012.
- [9] H. Wang, Y. Ge, J. Sun, H. Wang, N. Gu, Magnetic sensor based on image processing for dynamically tracking magnetic moment of single magnetic mesenchymal stem cell, *Biosens. Bioelectron.* 169 (2020), 112593, <https://doi.org/10.1016/j.bios.2020.112593>.
- [10] S.A. Nsibande, P.B.C. Forbes, Fluorescence detection of pesticides using quantum dot materials—a review, *Anal. Chim. Acta* 945 (2016) 9–22, <https://doi.org/10.1016/j.aca.2016.10.002>.
- [11] U. Resch-Genger, M. Grabolle, S. Cavaliere-Jaricot, R. Nitschke, T. Nann, Quantum dots versus organic dyes as fluorescent labels, *Nat. Methods* 5 (2008) 763–775, <https://doi.org/10.1038/nmeth.1248>.
- [12] S.A. Shaik, S. Sengupta, R.S. Varma, M.B. Gawande, A. Goswami, Syntheses of N-doped carbon quantum dots (NCQDs) from bioderived precursors: a timely update, *ACS Sustain. Chem. Eng.* 9 (2021) 3–49, <https://doi.org/10.1021/acssuschemeng.0c04727>.
- [13] I.V. Martynenko, A.P. Litvin, F. Purcell-Milton, A.V. Baranov, A.V. Fedorov, Y. K. Gun'ko, Application of semiconductor quantum dots in bioimaging and biosensing, *J. Mater. Chem. B* 5 (2017) 6701–6727, <https://doi.org/10.1039/C7TB01425B>.
- [14] F. Wu, H. Su, X. Zhu, K. Wang, Z. Zhang, W. Wong, Near-infrared emissive lanthanide hybridized carbon quantum dots for bioimaging applications, *J. Mater. Chem. B* 4 (2016) 6366–6372, <https://doi.org/10.1039/C6TB01646D>.
- [15] F. Wu, H. Su, K. Wang, W. Wong, X. Zhu, Facile synthesis of N-rich carbon quantum dots from porphyrins as efficient probes for bioimaging and biosensing in living cells, *Int. J. Nanomed.* 12 (2017) 7375–7391, <https://doi.org/10.2147/IJN.S147165>.
- [16] H. Su, Y. Liao, F. Wu, X. Sun, H. Liu, W. Kai, X. Zhu, Cetuximab-conjugated iodine doped carbon dots as a dual fluorescent/CT probe for targeted imaging of lung cancer cells, *Colloid Surf. B* 170 (2018) 194–200, <https://doi.org/10.1016/j.colsurfb.2018.06.014>.
- [17] L. Yue, H. Li, Q. Sun, J. Zhang, X. Zhu, Red-emissive ruthenium-containing carbon dots for bioimaging and photodynamic cancer therapy, *ACS Appl. Nano Mater.* 3 (2020) 869–876, <https://doi.org/10.1021/acsnanm.9b02394>.
- [18] Z. Zhang, G. Han, J. Zhao, R. Zhang, X. Tian, Z. Liu, A. Wang, R. Liu, B. Liu, M. Y. Han, Membrane-penetrating carbon quantum dots for imaging nucleic acid structures in live organisms, *Angew. Chem. Int. Ed.* 58 (2019) 7087–7091, <https://doi.org/10.1002/anie.201903005>.
- [19] Y. Cai, R. Tang, Nanotechnologies for the life sciences, *J. Mater. Chem.* 18 (2008) 3775–3787, <https://doi.org/10.1039/b805407j>.
- [20] D. Shao, M. Lu, D. Xu, X. Zheng, Y. Pan, Y. Song, J. Xu, M. Lie, M. Zhang, J. Li, G. Chi, L. Chen, B. Yang, Carbon dots for tracking and promoting the osteogenic differentiation of mesenchymal stem cells, *Biomater. Sci.* 5 (2017) 1820–1827, <https://doi.org/10.1039/c7bm00358g>.
- [21] T. Malina, K. Poláková, J. Skopalík, V. Milotová, R. Zboil, Carbon dots for in vivo fluorescence imaging of adipose tissue-derived mesenchymal stromal cells, *Carbon* 152 (2019) 434–443, <https://doi.org/10.1016/j.carbon.2019.05.061>.
- [22] H. Cai, J. Ma, X. Xu, H. Chu, D. Zhang, J. Li, Sulfonated glycosaminoglycan bioinspired carbon dots for effective cellular labeling and promotion of the differentiation of mesenchymal stem cells, *J. Mater. Chem. B* 8 (2020) 5655–5666, <https://doi.org/10.1039/D0TB00795A>.
- [23] J. Yan, S. Hou, Y. Yu, Q. Yong, T. Xiao, M. Yan, Z. Zhang, B. Wang, C.C. Huang, C. H. Lin, The effect of surface charge on the cytotoxicity and uptake of carbon quantum dots in human umbilical cord derived mesenchymal stem cells, *Colloids Surf. B* 171 (2018) 241–249, <https://doi.org/10.1016/j.colsurfb.2018.07.034>.
- [24] Y. Guo, C.C. Yan, P.F. Wang, L. Rao, C. Wang, Doping of carbon into boron nitride to get the increased adsorption ability for tetracycline from water by changing the pH of solution, *Chem. Eng. J.* 387 (2020), 124136, <https://doi.org/10.1016/j.cej.2020.124136>.
- [25] K.W. Piotr, W. Tomasz, B. Szczepan, W. Karolina, B.N. Volodymyrivna, B. Dariusz, Luminescence phenomena of carbon dots derived from citric acid and urea—a molecular insight, *Nanoscale* 10 (2018) 13889–13894, <https://doi.org/10.1039/c8nr03602k>.
- [26] Z. Zhang, L. Niu, X. Tang, R. Feng, G. Yao, W. Chen, W. Li, X. Feng, H. Chen, L. Sun, Mesenchymal stem cells prevent podocyte injury in lupus-prone B6.MRL-Faspr mice via polarizing macrophage into an anti-inflammatory phenotype, *Nephrol. Dial. Transpl.* 34 (2019) 597–605, <https://doi.org/10.1093/ndt/gfy195>.
- [27] C. Zhu, J. Zhai, S. Dong, Bifunctional fluorescent carbon nanodots: green synthesis via soy milk and application as metal-free electrocatalysts for oxygen reduction, *Chem. Commun.* 48 (2012) 9367–9369, <https://doi.org/10.1039/c2cc33844k>.
- [28] J. Liu, X.L. Liu, H.J. Luo, Y.F. Gao, One-step preparation of nitrogen-doped and surface-passivated carbon quantum dots with high quantum yield and excellent optical properties, *RSC Adv.* 4 (2014) 7648–7654, <https://doi.org/10.1039/c3ra47577h>.
- [29] W.S. Zou, Q.C. Zhao, J. Zhang, X.M. Chen, X.F. Wang, L. Zhao, S.H. Chen, Y. Q. Wang, Enhanced photoresponsive polyethyleneimine/citric acid cocarbonized dots for facile and selective sensing and intracellular imaging of cobalt ions at physiologic pH, *Anal. Chim. Acta* 970 (2017) 64–72, <https://doi.org/10.1016/j.aca.2017.03.018>.
- [30] D. Xu, L. Fang, H. Chen, L. Yin, S. Ying, J. Xie, One-step hydrothermal synthesis and optical properties of self-quenching-resistant carbon dots toward fluorescent ink and as nanosensors for Fe³⁺ detection, *RSC Adv.* 9 (2019) 8290–8299, <https://doi.org/10.1039/c8ra10570g>.
- [31] P. Li, X. Yang, X. Zhang, J. Pan, X. Xing, Surface chemistry-dependent antibacterial and antibiofilm activities of polyamine-functionalized carbon quantum dots, *J. Mater. Sci.* 55 (2020) 1–14, <https://doi.org/10.1007/s10853-020-05262-6>.
- [32] Z. Yang, M.H. Xu, Y. Liu, F.J. He, F. Gao, Y.J. Su, H. Wei, Y.F. Zhang, Nitrogen-doped, carbon-rich, highly photoluminescent carbon dots from ammonium citrate, *Nanoscale* 6 (2014) 1890–1895, <https://doi.org/10.1039/c3nr05380f>.
- [33] A.A. Strömstedt, L. Ringstad, A. Schmidtchen, M. Malmsten, Interaction between amphiphilic peptides and phospholipid membranes, *Curr. Opin. Colloid* 15 (2010) 467–478, <https://doi.org/10.1016/j.cocis.2010.05.006>.
- [34] M.C.Z. Kasuya, S. Nakano, R. Katayama, K. Hatanaka, Evaluation of the hydrophobicity of perfluoroalkyl chains in amphiphilic compounds that are incorporated into cell membrane, *J. Fluor. Chem.* 132 (2011) 202–206, <https://doi.org/10.1016/j.jfluchem.2011.01.004>.
- [35] H. Zhang, Y. Li, X. Liu, P. Liu, Y. Wang, T. An, H. Yang, D. Jing, H. Zhao, Determination of iodide via direct fluorescence quenching at nitrogen-doped carbon quantum dot fluorophores, *Environ. Sci. Technol. Lett.* 1 (2014) 87–91, <https://doi.org/10.1021/ez400137j>.
- [36] D. Wu, P. Ye, M. Wang, Y. Wei, X. Li, A. Xu, Cobalt nanoparticles encapsulated in nitrogen-rich carbon nanotubes as efficient catalysts for organic pollutants degradation via sulfite activation, *J. Hazard Mater.* 352 (2018) 148–156, <https://doi.org/10.1016/j.jhazmat.2018.03.040>.
- [37] G.T. Maribel, O.M. Guadalupe, G.J. Cruz, G.L. Ma, S.M. Víctor, G.S. Francisco, XPS study of the chemical structure of plasma biocopolymers of pyrrole and ethylene glycol, *Adv. Chem.* 2014 (2014) 1–8, <https://doi.org/10.1155/2014/965920>.